AFRL-AFOSR-VA-TR-2023-0023

Carbon oxidation in extreme environments

Alexandre Martin
KENTUCKY UNIV LEXINGTON
201 KINKEAD HALL
LEXINGTON, KY, 40506 - 0001
US

10/05/2022
Final Technical Report

Air Force Research Laboratory
Air Force Office of Scientific Research
Arlington, Virginia 22203
Air Force Materiel Command

REPORT DOCUMENTATION PAGE

PLEASE DO NOT RETURN YOUR FORM TO THE ABOVE ORGANIZATION.

1. REPORT DATE	2. REPORT TYPE	3. DATES COVERED	
20221005	Final	START DATE 20180815	END DATE 20210814

4. TITLE AND SUBTITLE
Carbon oxidation in extreme environments

5a. CONTRACT NUMBER	5b. GRANT NUMBER	5c. PROGRAM ELEMENT NUMBER
	FA9550-18-1-0261	61102F
5d. PROJECT NUMBER	**5e. TASK NUMBER**	**5f. WORK UNIT NUMBER**

6. AUTHOR(S)
Alexandre Martin

7. PERFORMING ORGANIZATION NAME(S) AND ADDRESS(ES)
KENTUCKY UNIV LEXINGTON
201 KINKEAD HALL
LEXINGTON, KY 40506 - 0001
US

8. PERFORMING ORGANIZATION REPORT NUMBER

9. SPONSORING/MONITORING AGENCY NAME(S) AND ADDRESS(ES)	10. SPONSOR/MONITOR'S ACRONYM(S)	11. SPONSOR/MONITOR'S REPORT NUMBER(S)
Air Force Office of Scientific Research 875 N. Randolph St. Room 3112 Arlington, VA 22203	AFRL/AFOSR RTA1	AFRL-AFOSR-VA-TR-2023-0023

12. DISTRIBUTION/AVAILABILITY STATEMENT
A Distribution Unlimited: PB Public Release

13. SUPPLEMENTARY NOTES

14. ABSTRACT
Hypersonic aircrafts must be protected from the extremely high temperatures of the gas impinging their surface. This is achieve by using Thermal Protection Systems (TPS), which typically consist of a thin coating layer made of a very resistant material that stands well these high temperatures. One of the most versatile materials used for this purpose is carbon, in some of its many possible forms, such as graphite, glassy or amorphous. However, in the presence of high temperature oxygen, as is the case during flight, the carbon layer of the TPS degrades and the solid carbon become gaseous CO and CO2. As a result, the protective layer may eventually disappear, leaving the vehicle without protection. Thus, a good understanding of its behavior under these conditions is very important to improve the safety of hypersonic flights. The guiding idea of this project is to study carbon oxidation in these extreme conditions, from a fundamental point of view. This will be achieved by examining the details of the atomicscale processes that ultimately govern the loss of carbon from the TPS. After hitting the surface, oxygen atoms remain wandering across the TPS surface until they connect to weakly attached carbon atoms .

15. SUBJECT TERMS

16. SECURITY CLASSIFICATION OF:			17. LIMITATION OF ABSTRACT	18. NUMBER OF PAGES
a. REPORT U	b. ABSTRACT U	c. THIS PAGE U	UU	2

19a. NAME OF RESPONSIBLE PERSON	19b. PHONE NUMBER *(Include area code)*
SARAH POPKIN	000-0000

AFOSR Grant FA9550-18-1-0261

Section 2: Technical Report

PI: Alexandre Martin

1 Accomplishments

In the proposal of this project, the following four specific objectives had been outlined:

1. **Objective 1:** Identify and characterize the species and elementary atomic reactions of carbon oxidation
2. **Objective 2:** Integrate them into a comprehensive, molecular-scale kinetic mechanism of carbon materials
3. **Objective 3:** Develop models accounting for the development of surface roughness due to oxidation
4. **Objective 4:** Integrate these results in a hypersonic aerothermodynamic CFD code to model the interaction of the non-equilibrium gaseous boundary layer with the ablating carbonaceous surface

Our proposed approach to achieve these objectives contains these three distinct tasks:

- **Task A:** Comprehensive atomistic mechanism of carbon oxidation (Objective 1 and 2)
- **Task B:** Mesoscale mechanism and roughness development models (Objective 3)
- **Task C:** Gas boundary layer — ablating carbon surface interaction (Objective 4)

In the following, the accomplishments within each of these three tasks are presented, and necessary details are provided.

1.1 Task A

The goal of Task A is the construction of a comprehensive, atomic-scale mechanism for the oxidation of carbon surfaces, based on first principles. We started out this task with a comprehensive literature review on computational studies of carbon oxidation. In particular, we found early studies were using molecular orbital theory [1–4] to calculate the intrinsic oxidation rates of different kinds of carbon edge species occupied with oxygen adsorbates. More recently, the more accurate Density Functional Theory (DFT) method has been utilized for that same purpose [5–17], albeit on various levels of DFT theory.

The first direct outcome of this activity, which is related to the Objective 1, was the identification of the oxygen surface species that are relevant to the oxidation reaction. These species are listed in Figure 1. Furthermore, we were able to extract a set of elementary surface reactions on the carbon surface. Those include the adsorption of atomic and molecular oxygen on the carbon surface, in

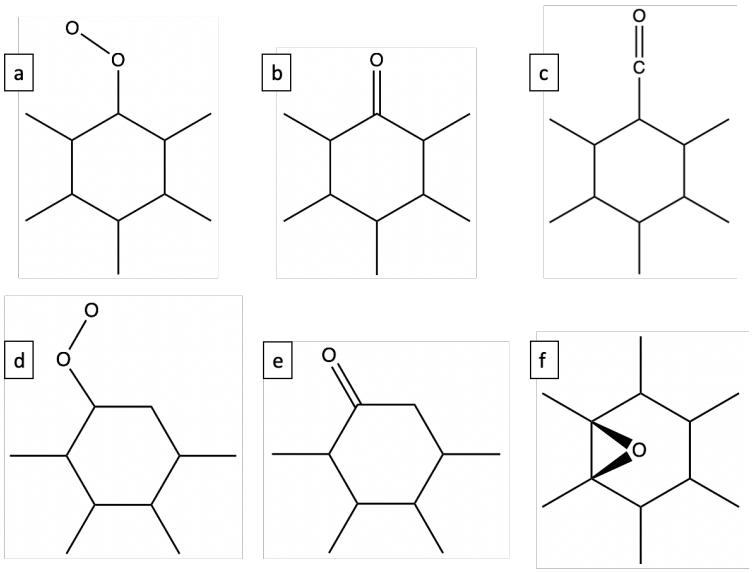

Figure 1: *Adsorbed oxygen surface species: molecular oxygen adsorbed to zigzag edge $O_{2,zz}$ (a), zigzag semiquinone (b), ketone (c), molecular oxygen adsorbed to armchair edge $O_{2,ac}$ (d), armchair semiquinone (e), epoxide (f).*

the latter case followed by the dissociation of the molecular oxygen adsorbate, diffusion of oxygen adsorbates across the surface, as well as desorption of oxygen itself and CO as a result of an oxidation reaction. All these reactions are listed in Table 1.

Table 1: *Kinetic reaction mechanism for carbon oxidation where rate* $k = A\exp\left(-E_a/k_BT\right)$

#	Reaction	$A\,(\mathrm{s}^{-1})$	E_a (eV)	Reference
ADS1	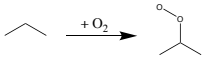	$\frac{P_O A_{eff}}{\sqrt{2\pi m_{O_2} k_B T}}$	0.000	[6, 11]
ADS2	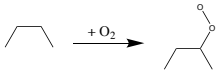	$\frac{P_O A_{eff}}{\sqrt{2\pi m_{O_2} k_B T}}$	0.311	[5, 10]
ADS3	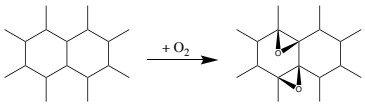	$\frac{P_O A_{eff}}{\sqrt{2\pi m_{O_2} k_B T}}$	1.700	[12]
ADS4	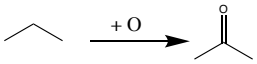	$\frac{P_O A_{eff}}{\sqrt{2\pi m_O k_B T}}$	0.0	[17]
ADS5	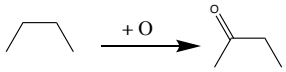	$\frac{P_O A_{eff}}{\sqrt{2\pi m_O k_B T}}$	0.0	[17]
ADS6	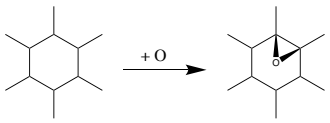	$\frac{P_O A_{eff}}{\sqrt{2\pi m_O k_B T}}$	0.0	[17]
ADS7	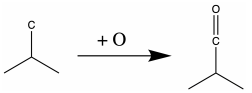	$\frac{P_O A_{eff}}{\sqrt{2\pi m_O k_B T}}$	0.0	[17]
DIS1	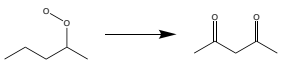	3.6×10^{12}	0.041	[6, 11]

DIS2	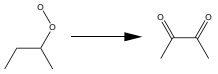	1.5×10^{12}	0.694 [5]
DIS3	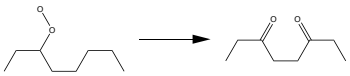	3.5×10^{12}	0.238 [10]
DIS4	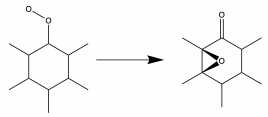	1.2×10^{12}	1.513 [11]
DIFF1	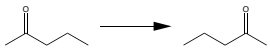	5.4×10^{12}	1.904 [6,8]
DIFF2	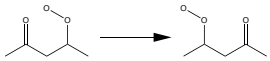	3.0×10^{11}	0.943 [11]
DIFF3	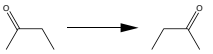	4.3×10^{12}	1.399 [8]
DIFF4	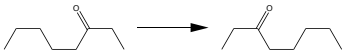	3.4×10^{13}	1.275 [8]
DIFF5	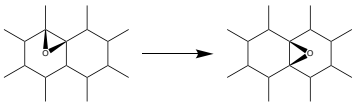	1.0×10^{13}	0.730 [12]
DIFF6	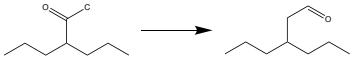	4.3×10^{12}	1.399 [8]
DIFF7		5.4×10^{12}	1.904 [6,8]
DIFF8	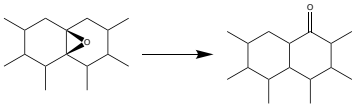	1.0×10^{13}	0.730 [12]
DIFF9	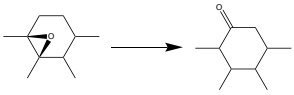	1.0×10^{13}	0.730 [12]
DIFF10	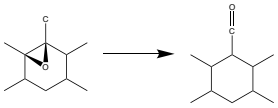	1.0×10^{13}	0.730 [12]
DIFF11	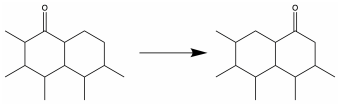	5.4×10^{12}	1.904 [6,8]
DIFF12	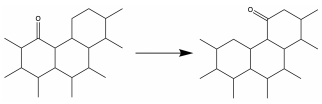	3.4×10^{13}	1.275 [8]
DIFF13	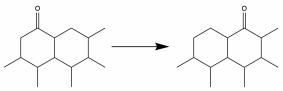	5.4×10^{12}	1.904 [6,8]
DIFF14	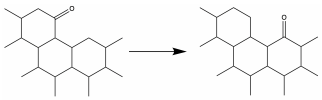	3.4×10^{13}	1.275 [8]
DIFF15	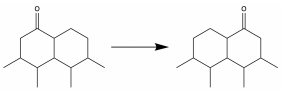	5.4×10^{12}	1.904 [6,8]
DES1	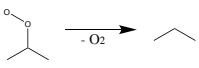	1.3×10^{14}	1.420 [11]

DES2	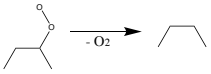	6.4×10^{14}	1.104	[5, 10]
DES3	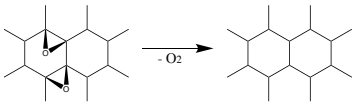	1.0×10^{13}	1.130	[12]
OXzz1	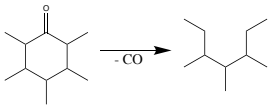	1.2×10^{16}	3.622	[2, 8]
OXzz2	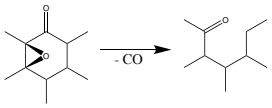	1.2×10^{16}	2.300	[2, 8]
OXzz3	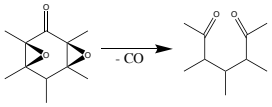	1.2×10^{16}	2.300	[2, 8]
OXac1	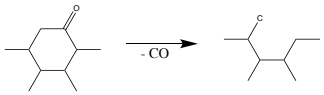	1.0×10^{13}	2.743	[2]
OXac2	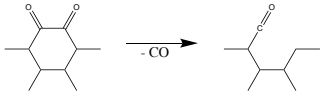	1.0×10^{13}	1.704	[2]
OXac3	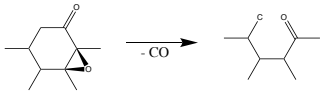	1.0×10^{13}	1.829	[2]
OXac4	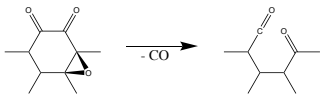	1.0×10^{13}	1.136	[2]
OXac5	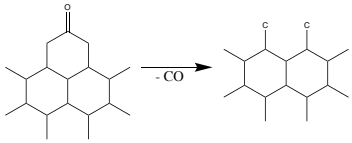	1.0×10^{13}	2.743	[2]
OXac6	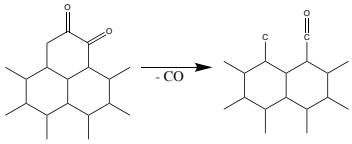	1.0×10^{13}	1.704	[2]
OXac7	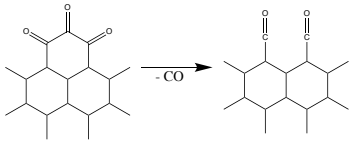	1.0×10^{13}	1.704	[2]
OXd1	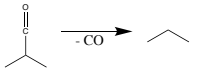	1.0×10^{13}	2.170	[14]
OXd2	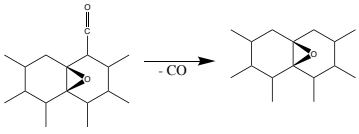	1.0×10^{13}	0.447	[14]
OXd3	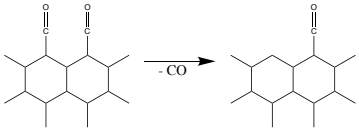	1.0×10^{13}	1.227	[14]

OXd4	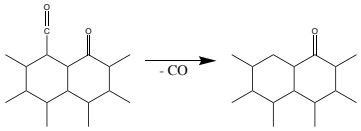	1.0×10^{13}	1.860	[14]
OXd5	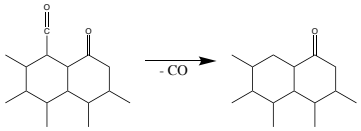	1.0×10^{13}	1.860	[14]
OXd6	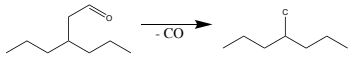	1.0×10^{13}	1.704	[2]
OXd7	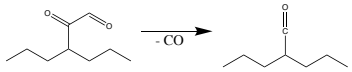	1.0×10^{13}	1.829	[2]

Notice that every elementary reaction comes with an associated elementary rate constant k. Those rate constant are derived on the basis of Transition State Theory (TST). TST allows the derivation of quantitative rate data such as activation energies E_A for elementary reactions from first principles. This is done by analyzing the atomic energies of reactant-, transition- and product-states on the potential energy surface (PES) of the reacting carbon surface.

To put this into perspective, this newly developed mechanism (Objective 2) differs in a number of ways from conventional oxidation mechanisms used in finite-rate chemistry solvers. First, it contains only elementary surface reactions, and those have rate constants derived from first principles. Hence, this new mechanism is universal in the sense that it is widely applicable to any reaction conditions, and for any graphitic carbon material. Second, this new mechanism is sterically resolved on the atomic level, which means that reactions are sensitive to the local atomic configuration. This is the key property that is used within Task B to simulate the actual evolution of the carbon surface on the atomic level. In contrast, conventional mechanism are to varying degrees phenomenological, with parameters that are adjusted to specific experimental conditions. Furthermore, they only include chemical reactions from a global perspective, often times relying on intermediate reaction steps that do not correlate with the elementary reactions on the atomic level on the surface.

In summary, all the efforts undertaken within Task A culminated in the comprehensive kinetic mechanism listed in Table 1, which accomplishes the Objectives 1 and 2 of this project.

1.2 Task B

Task B focuses on the study of the surface evolution of carbon surfaces during oxidation, and therefore directly addressing Objective 3. As early as 1926 [18], it has been found experimentally that on the mesoscopic level, characteristic pitys form on carbon surfaces during oxidation. Conceptually, this has been long explained to be the result of preferential removal of carbon atoms from so-called edge carbons on the surface. Those already are missing neighboring atoms in the hexagonal graphene layer, for instance due to naturally existing vacancy defects in the carbon surface structure. The relative lack of bonds causes the bonding energy of edge carbons to be lower, which ultimately facilitates removal by oxidation reactions. However, quantitative data on pitting through carbon oxidation has heretofore only been generated from experiments, and many of the dynamic features of pitting have not yet been revealed.

The first goal in Task B was therefore to be able to simulate and analyze pitting from the atomic

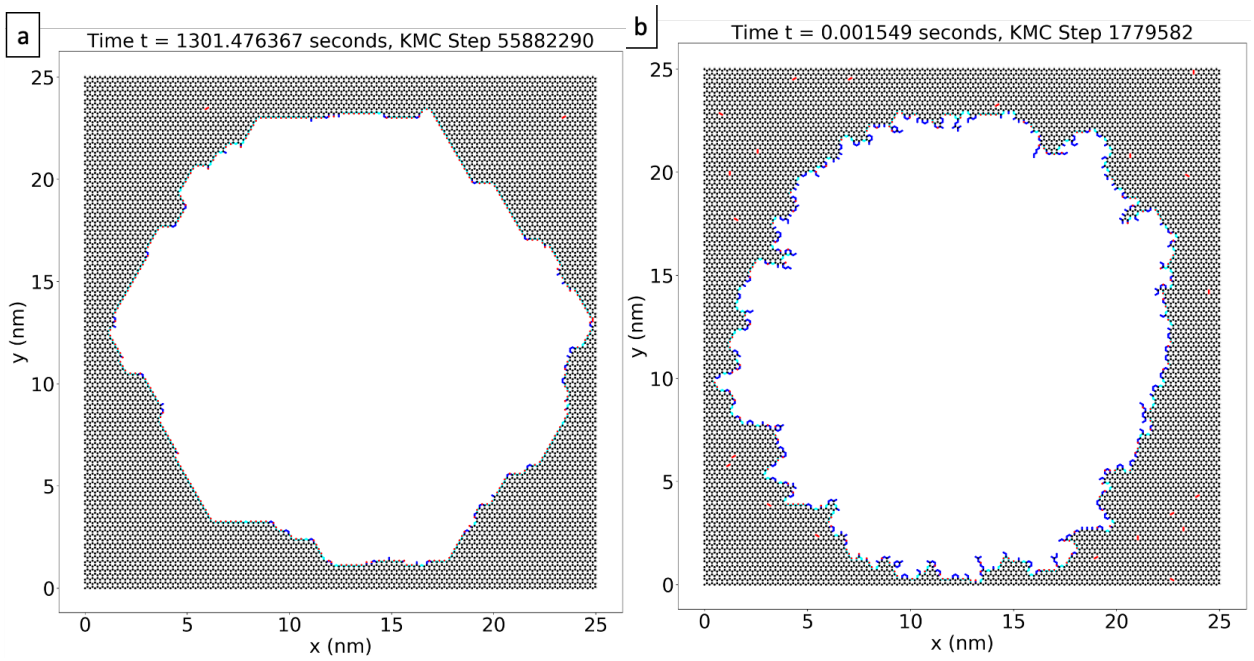

Figure 2: *Geometry comparison of simulated etch pits: hexagonal shape with smooth zigzag carbon edges at* $T = 850\,\mathrm{K}$, $P = 0.01\,\mathrm{mbar}$ *(a); circular shape with rough carbon edges at* $T = 1500\,\mathrm{K}$, $P = 100\,\mathrm{mbar}$ *(b). A full videos of these simulations are provided as Supplementary Video SV2 (a) and Supplementary Video SV3 (b).*

level. This has been achieved by implementing the kinetic mechanism developed in Task A in a Kinetic Monte Carlo (KMC) computational framework. In short, KMC is a probabilistic method that simulates rare events, such as our elementary surface reactions, instead of atomic motion itself [19]. This allows it to simulate fairly large systems (graphene sheets with up to 100 nanometers in side length) too much longer times (up to seconds) than deterministic atomic methods such as molecular dynamics could do. The KMC code used for this work is called Zacros [20, 21]. It is a lattice based KMC code, which means that the surface graphene layer is directly represented as a hexagonal lattice. The kinetic mechanism is then implemented, where each elementary surface reaction corresponds to a local transformation of the states of select surface sites. The overall carbon oxidation reaction is ultimately simulated as a chain of those elementary reactions.

To demonstrate the capabilities of this simulation framework, two snapshots of oxidized graphene are shown in Figure 2. While a pit with atomically smooth edges, and overall hexagonal shape is oxidized at lower temperatures and pressures, the pits become circular with a certain degree of roughness along the edge at higher temperatures and pressure. This matches experimental behavior. Ref. [22] have observed a transition from hexagonal to circular pits with increasing temperature, and Ref. [23] have observed a transition from hexagonal to circular pits with increasing pressure. Interestingly, the hexagonal pitting regime is of interest for manufacturing graphene nanodevices. Atomically smooth edges in graphene are mostly required to ensure performance of such devices, and oxidative etching has been proposed as one potential manufacturing technique that can produce such edge configurations. Movies of these simulations can be found at:

- https://youtu.be/NVLgffbNgHo

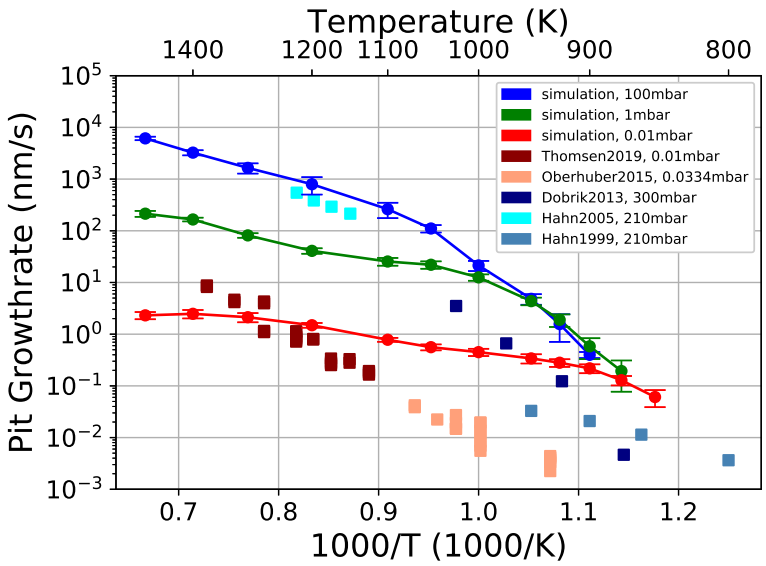

Figure 3: *Pit growth rates as a function of temperature and pressure. The errorbars correspond to the standard deviation between all simulated trajectories for each case. Experimental pit growth rates are included with squared boxes. The reference keys are Thomsen2019 [23], Oberhuber2015 [24], Dobrik2013 [25], Hahn2005 [26], Hahn1999 [27].*

- https://youtu.be/FENBgP6lL4o

We have also studied the dynamics of the pitting process. In accordance with experiments, we have found that the radius of a pit is growing at a constant rate in time at constant reaction conditions. This pit growthrate is a function of both pressure and temperature, as can be seen in Figure 3. A few interesting things can be noted here, as the behavior of the simulation curves relate to reaction balances. First, the three pressures curves are collapsing together at low temperatures. In that reaction regime, the overall oxidation reaction is rate limited by the elementary surface oxidation reactions. In fact, looking at Figure 4, one can see that the oxygen coverage of edge carbons in that regime is high. This is due to the fact that oxygen from the gas phase adsorbs faster to the carbon surface than oxidation reactions can remove those oxygen adsorbates (and carbon atoms). At higher temperatures, the rate of oxidation reactions increases faster relative to the adsorption reactions. Hence, the pressure starts to play a role in the pit growthrate. And equally, the edge coverage starts to drop significantly, until it reaches essentially zero coverages at very large temperatures. The rate limiting factor in this regime is the adsorption of gaseous oxygen, which is directly proportional to the pressure.

As has been shown, this novel KMC simulation framework allows for the first time to study the evolution of oxidizing carbon surfaces, at relevant pressures, temperatures, time- and lengthscales for hypersonic applications.

1.3 Task C

Objective 4 of this project, addressed through this task, is to close the loop on the multi-scale approach an integrate the results of Task B in a hypersonic aerothermodynamic CFD code to model the interaction of the non-equilibrium gaseous boundary layer with the ablating carbonaceous

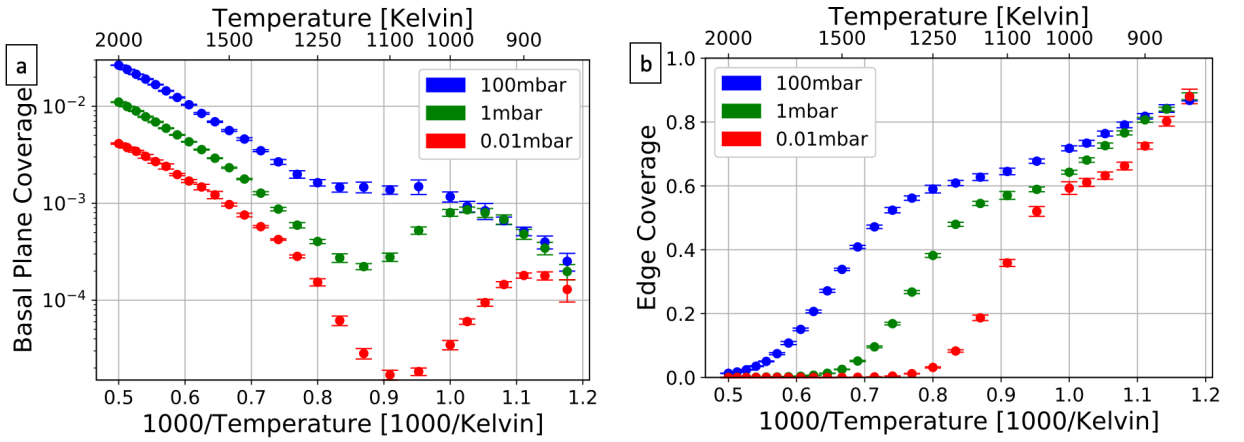

Figure 4: *Oxygen coverage of the basal plane (a) and edge sites (b) as functions of temperature and pressure. The errorbars correspond to the standard deviation between all simulated trajectories for each case.*

surface. This was achieved in two steps: first, the hypersonic aerothermodynamic CFD code KATS was updated to take into account non-uniform surface recession, using a novel method, and second, the surface boundary condition was updated to allow finite-rate chemistry rate

1.3.1 Universal Solver with immersed boundary method

Modeling the interactions between porous flow and pure flow at atmospheric entry conditions is a challenging task. New models and high fidelity numerical tools are required to better understand porous material and aerothermal flow interactions for ablation problems. To tackle this problem, a unified solver that treats both domains at the same time is developed based on Volume Averaged Navier-Stokes equations. The solver adopts a universal system of equations that covers plain and porous flows with reactions. [28, 29] The developed framework is the key foundation of the macro-scale simulation of carbon oxidation.

To resolve the arbitrary interface of the fluid-solid interaction, a new method is developed. With this method, the fluxes through the computational faces are controlled using a so-called "hinge" matrix. The method is simple to implement and is comparable in accuracy to other immersed boundary methods, such as the Cartesian grid method. The hinge method is verified by solving a low-speed flow in an irregular domain. Figure 5(a) shows a 2D flow domain of 0.1 m $\times$ 0.5 m, with two half circle voids at (0.2, 0) m and (0.3, 0.1) m. The flow is set to be pure nitrogen. An inflow velocity of 0.1 m/s is set at the front surface ($x = 0$ m) and a pressure outlet is set at the back wall ($x = 0.5$ m). The rest of the boundary conditions are walls. Figure 5(b) shows the exact boundary conditions by using hinge value to mimic the voids inside the domain. The two half-circle voids are now represented by the hinge parameter with a value of zero. The calculation is running to the steady-state solution when the total tolerance of 1×10^{-8} is reached.

Figure 6(a) displays the contours of velocity magnitude over the entire domain. It can be seen that because of the voids, the flow accelerates when it travels through the middle channel, it reaches its maximum speed. Figure 6(c) show the directional components of the velocity field. Data are extracted at the centerline ($y = 0.05$ m) for both methods to better compare the accuracy.

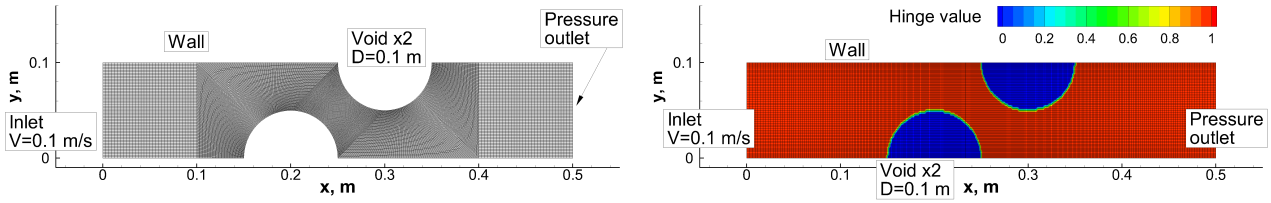

(a) Computational base grid **(b)** Hinge value

Figure 5: *Velocity contours and directional components*

Figure 6(b) shows the comparison of velocity magnitude. It can be seen that solutions from the newly proposed method have an excellent agreement with the traditional CFD solution. Figure 6(d) compares the results for directional velocity component.

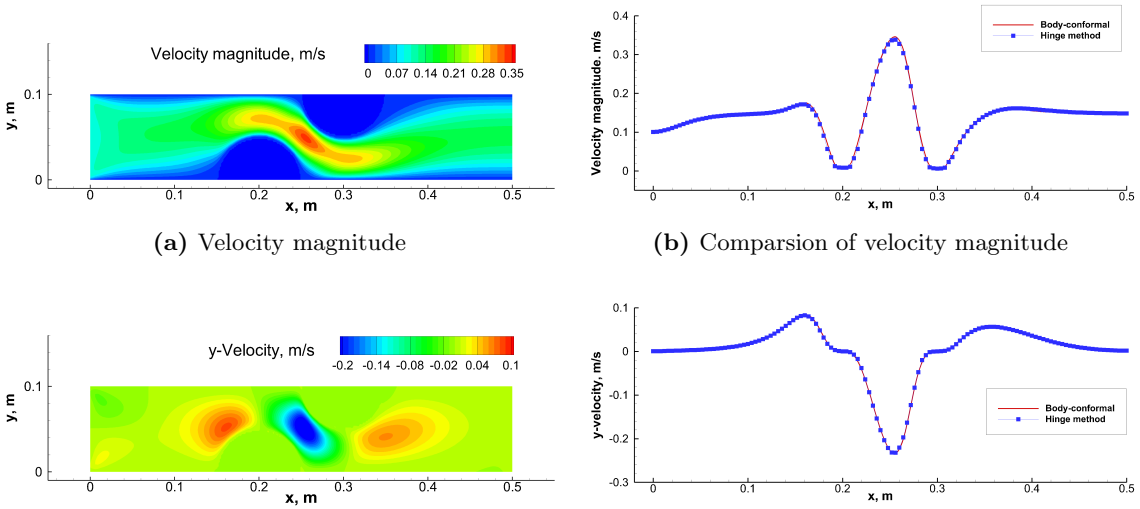

(a) Velocity magnitude **(b)** Comparsion of velocity magnitude

(c) y-Velocity magnitude **(d)** Comparsion of $y-$velocity

Figure 6: *Velocity contours and directional components*

Pitting Modeling - Material Response To model the damage of oxidation on carbon fiber, a pitting model is developed based on the Hinge method. A demonstration case is shown as in Fig. 7a, where a constant heat flux is imposed at the inner wall of the hole with a re-radiative condition. Figure 7b shows the evolution of temperature within the first 0.3 second. At $t = 0.05$ s, the temperature starts to increase at the inner wall. As the temperature hits the oxidation threshold, the inner wall starts to oxidize. The resultant residue shapes of the material become very irregular since the pits can grow large to connect with others and form a larger pit. Figure 7c presents an application of such model to a cylindrical fiber geometry. The fiber starts to heat up rapidly because of its low conductivity and high external heat flux. At $t = 0.004$ s, the surface begins to oxidize at various locations. At $t = 0.007$ s, surface pitting has penetrated the entire fiber and then cause this fiber to fail. At the final step when $t = 0.008$ s, a very large portion of the solid has been oxidized away and the residues are highly irregular. It can be observed that the oxidation is very sensitive to the surface roughness parameter.

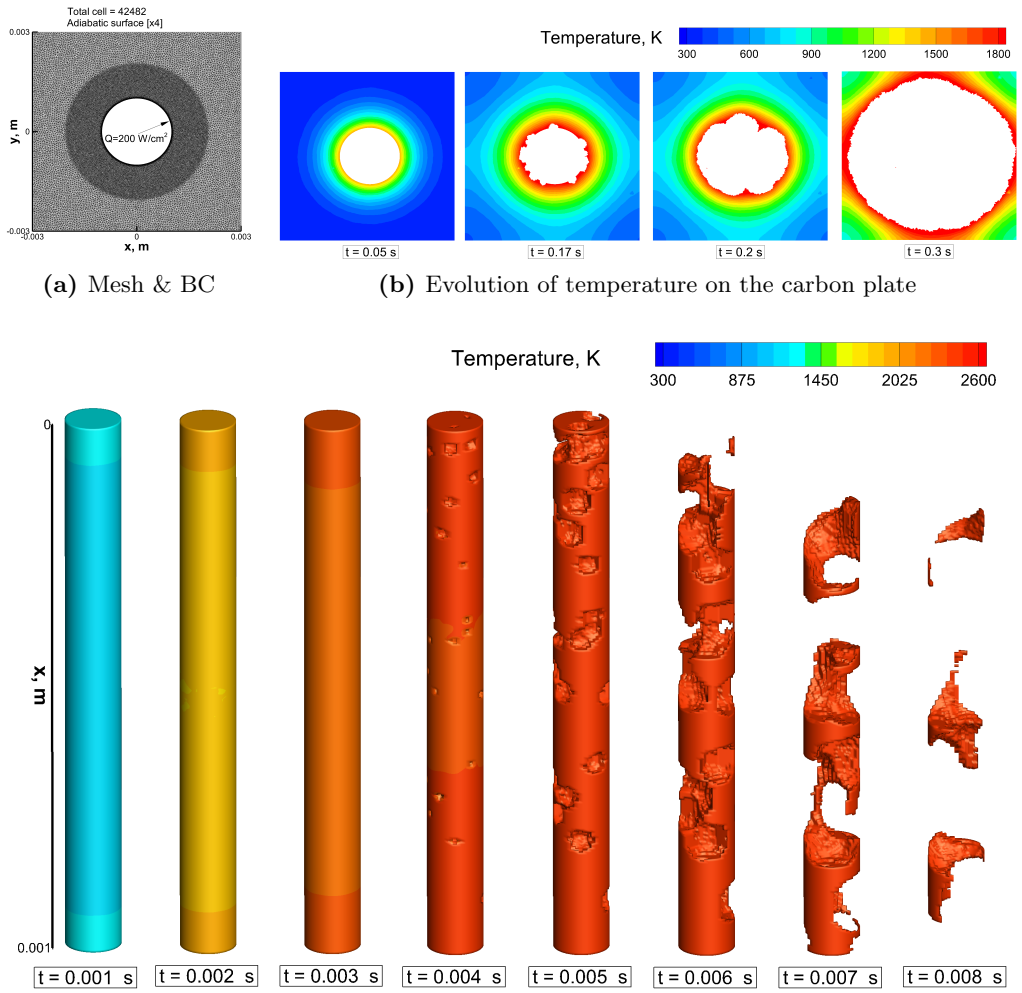

(a) Mesh & BC

(b) Evolution of temperature on the carbon plate

(c) Evolution of temperature and surface pitting on a single fiber

Figure 7: *Carbon fiber surface pitting model.*

Macro-scale Modeling – Conjugate Heat Transfer Boundary Condition The concept of conjugate heat transfer refers to the fact that in most cases, the heat transfer happens in both the fluid and solid at the same time when there is a temperature difference at the interface. In most cases, heat conduction will dominate the heat transfer in solids and the combination of conduction and convection will dominate the fluid. Figure 8a shows the computational grid, which is a structured mesh with 128×512 cells. For the fluid domain, at $x = 0$ m is the inlet, where a fixed velocity is set to be [1, 0, 0] m/s and a temperature is 400 K. For solid, three adiabatic walls are set, where no heat exchange is allowed. Figure 8 shows the evolution of temperature at different time steps for both fluid and solid domains. When $t = 25$ s, a clear thermal boundary layer has already formed from the interface, where the fluid is cooled due to the cold wall. The temperature of the solid gradually increases, and at the left ($x = 0$ m), the temperature rises most since that region contacts the 'hot' fluid first. When $t = 100$ s, shown in Fig. 8c, the temperature field in the solid becomes more uniform. The thermal boundary layer in the fluid domain becomes thinner since the rising temperature of the interface. The results clearly show that the Hinge method has successfully captured the transient response of the conjugate heat transfer between the fluid and

solid.

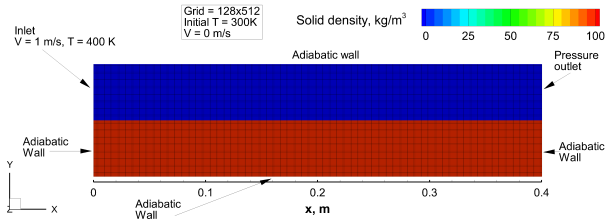

(a) Computational grid and boundary conditions for conjugate heat transfer case.

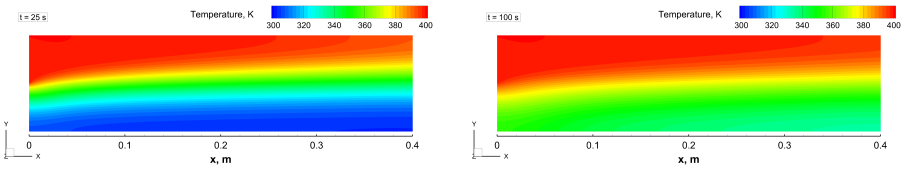

(b) $t = 25$ s **(c)** $t = 100$ s

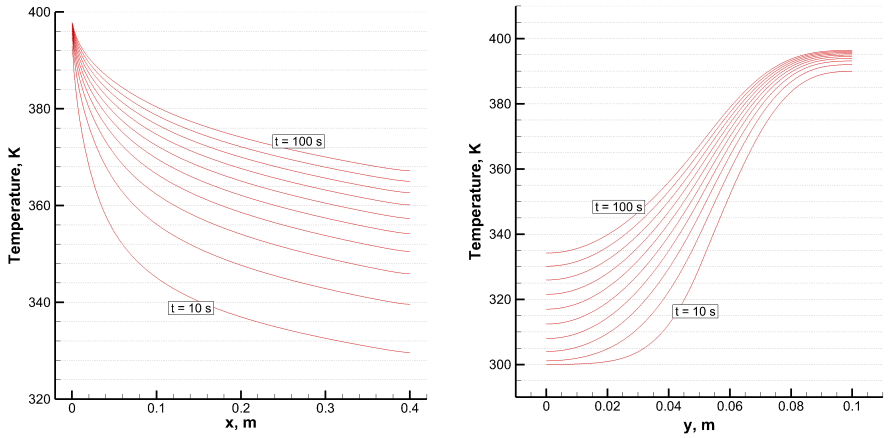

(d) Temperature history at the interface ($y = 0.05$ m) **(e)** Temperature history at the end wall ($x = 0.4$ m)

Figure 8: *The evolution of temperature distribution for both the fluid and solid.*

Macro-Scale Recession - Unsteady laminar flow In this case, the Hinge method has been applied to simulate the solid sublimation in a fluid. Figure 9a shows the details of the case setup. Figure 9 displays the evolution of temperature and velocity magnitude for this case. At $t = 1$ s, the high-temperature fluid has already caused the solid to sublimate, shown in Fig. 9b. It can be seen that the rectangle solid has lost its left corner region, forming a smooth curve, indicated by the black solid line. As a result, the hot fluid has been cooled down near the solid, where a thermal boundary layer is formed. Figure 9c shows the velocity magnitude with the streamlines at this time step. Because the channel becomes narrower over the solid, the velocity increases as expected. At $t = 4$ s, the sublimation has caused the solid to lose the original shape and forms a smooth elliptic outline, shown in Fig. 9d. As a result, the channel becomes wider than the previous time step, and the flow field changes accordingly. At $t = 7$ s, the solid material keeps losing its mass due to the sublimation, and only a very small fraction of the original shape remains in the channel, shown in Fig. 9f. The results demonstrate the capability of the developed Hinge method

for handling changing and deforming fluid-solid interface by using the dynamic hinge vector.

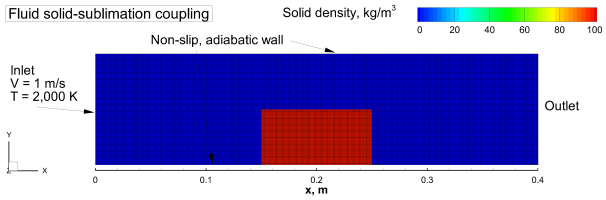

(a) Computational grid, domain setup and boundary conditions for solid sublimation case.

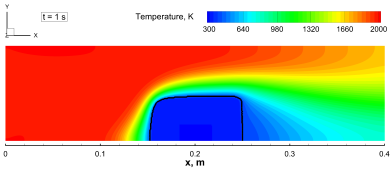

(b) Temperature at $t = 1$ s

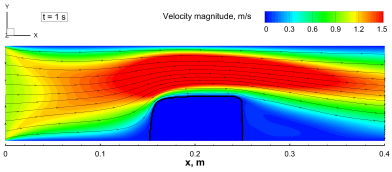

(c) Velocity magnitude at $t = 1$ s

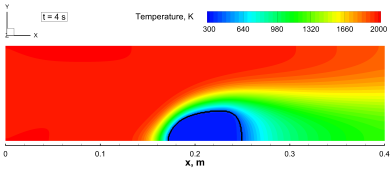

(d) Temperature at $t = 4$ s

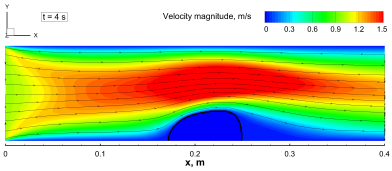

(e) Velocity magnitude at $t = 4$ s

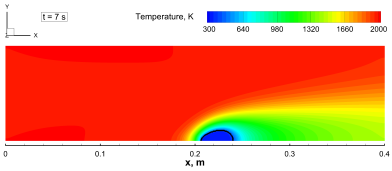

(f) Temperature at $t = 7$ s

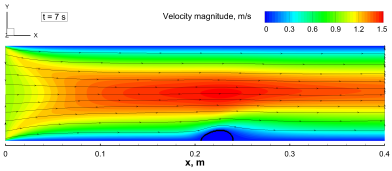

(g) Velocity magnitude at $t = 7$ s

Figure 9: *The evolution results of Temperature and velocity magnitude distribution for solid sublimation case.*

Macro-Scale Recession - Hypersonic flow Modeling ablating surfaces in the hypersonic regime has been – and still remain – a challenge. It is a two-way coupling process: the fluid causes the solid interface to deform and react, while the changing surface causes the flow field near the interface to behave very differently. It is critical to model the changing shape of the fluid-solid interface, the material response of the solid, the changing boundary layer flow near the interface; all of these form a strongly coupled solution. This case serves as an initial study of the fluid-ablation interaction modeling of a hypersonic case and shows the capability of the proposed Hinge method.

Figure 10(a) shows the hinge value distribution and computational grid for the nose of the IRV2 vehicle, in a 0.3×0.3 m^2 area. A Cartesian grid of 256×256 is used with a refinement near the front part. The simulation starts with an inlet speed of 2,000 m/s at $x = 0$ m and reaches a steady-state solution at approximately 40% of the entire simulation. In this preliminary stage, the fluid is set to be non-reacting pure nitrogen with constant properties. Figure 10(b) presents the velocity and temperature contours. It can be seen that a detached bow shock is formed and captured by the calculation, with a stagnation point at the very front nose. Temperature shows a similar pattern, with the highest value of approximately 2,500 K at the stagnation point. The aerodynamic heating on the solid surface is also captured - it can be observed that at the interface, the temperature reaches around 2,000 K. Figure 10(c) displays the pressure and density distribution of the steady-state solution. It can be observed that very pressure and density follow the pattern of the velocity field, with a maximum value at the stagnation point. It should be noted that at this preliminary stage, the solid part, which is represented by a hinge value of 0, is assumed to be void. That is the

reason the temperature does not transfer into the material as well as the density is the same as the initial condition.

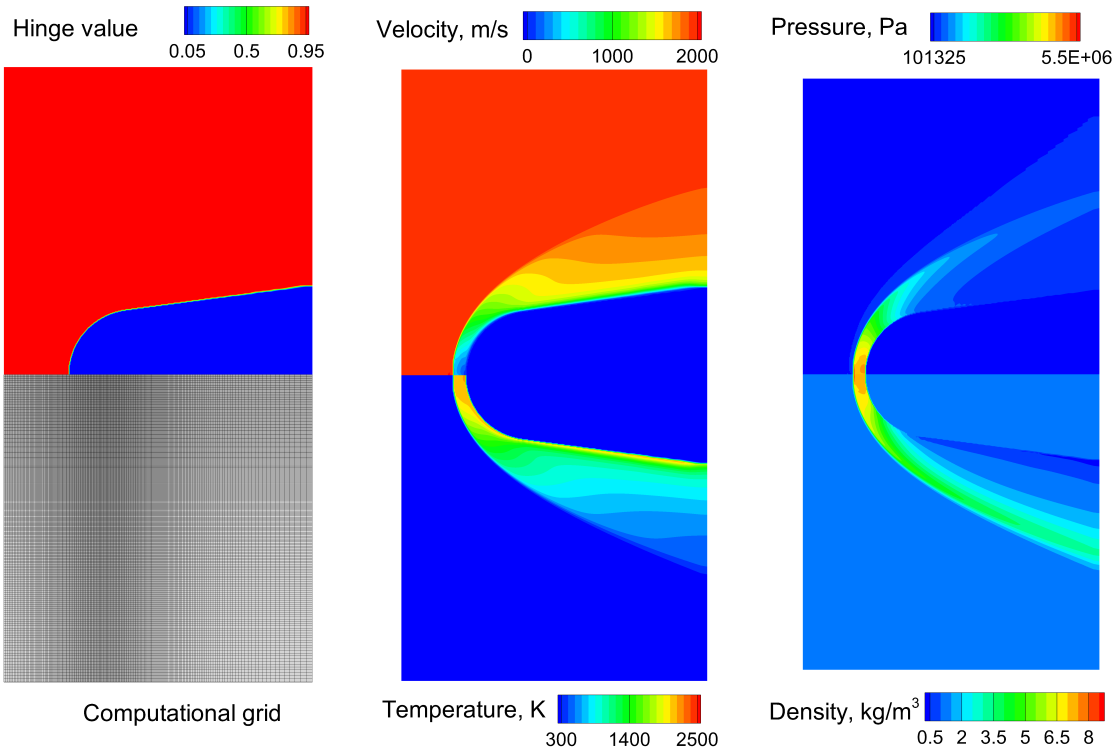

(a) Hinge value and computational grid **(b)** Velocity and temperature **(c)** Pressure and density

Figure 10: *Hypersonic modeling - IRV2 vehicle*

To illustrate how the changing interface impacts the flow field, the damage is manually generated at the surface, in the forms of spherical holes – or pits. Figure 11(a) displays the flow field as the holes become large enough to be visible, with the black solid line outlining the original location of the solid interface. The same pattern can be seen at the final step, shown in Fig. 11(c), where the pits grow much larger. Unlike the velocity, at the edge of the larger pit, it can be seen that higher temperature occurs due to the surface holes. The newly damaged surfaces, which are set to be adiabatic walls, create space that traps the air, leading to a new stagnation point so that the temperature becomes higher than a normal surface. In the final version of this paper, the ablating surface module will be added to this case, and that will also affect the external boundary layer.

1.3.2 Surface Oxidation of Carbon/Carbon Composites

As a first step towards implementing the chemistry model obtained in Task B, a reference model – the so-called MURI model – was implemented into KATS. [30] The MURI model was build exclusively using molecular beam experimental results. The model is simple to implement, and is able to provide species production and surface recession based on physical process rather than assumed relationship between mass and heat transfer, such as is the case when using legacy film coefficients models. Using this model, baseline analysis of the influence of site densities on the ablation rate were performed.

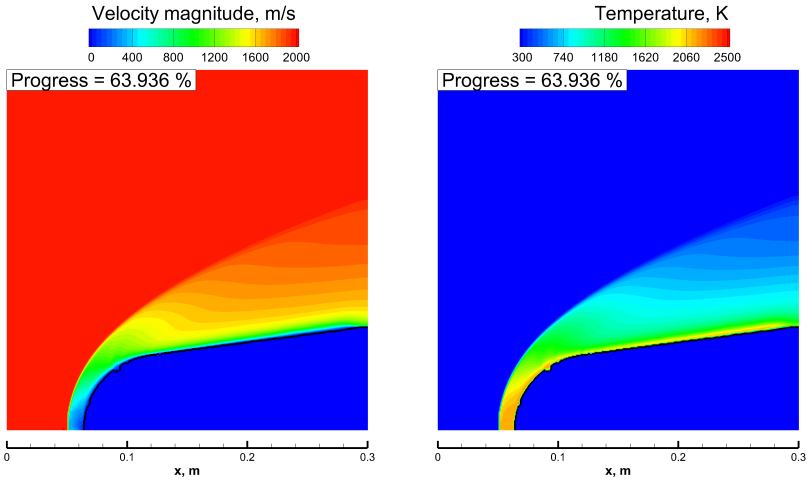

(a) Three pitting initiated **(b)** Three pitting initiated

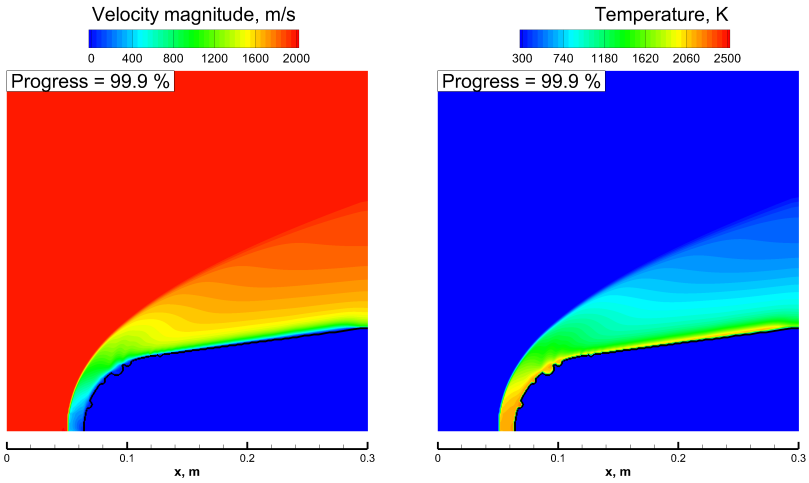

(c) Pitting grow and becomes larger **(d)** Pitting grow and becomes larger

Figure 11: *Fluid-ablation interactions, where holes are generated at the surfaces to affect the flow*

The total number of reaction sites B in surface oxidation model is considered an important parameter. A surface site concentration of $B = 1 \times 10^{-5}$ mol/m^2 is typically assumed. This value is based on the number of carbon atoms per surface area of graphite lattice [31]. However, it may be affected by the manufacturing processes of the surface ablator.

One of the finding of this study is that the ablation process is independent of the the number of sites if the reactions rates can reach steady-state. However, when implemented in a CFD code, these reactions are limited by the time-step used, and might not immediately reach that state. In such case, variation in species mass fluxes between different total surface site density values are found. This results provide the expected range of validity, and can lead to the construction of an oxidation model independent of the total surface site density.

The following results are obtained by performing a CFD simulation of a 8 degree sphere cone with 1500 K isothermal wall at 40 km altitude with the freestream condition shown in Table 2.

Table 2: *Free-stream conditions for 40 km case*

T_∞, K	$T_{v\infty}$, K	ρ_∞, kg/m^3	V_∞, m/s
250.349	250.349	3.5424×10^{-4}	7000.0

Figure 12a shows the mass flux of the surface reacting species along the surface of the vehicle. When assuming that surface chemistry reaches steady state values during each CFD time-step, it can observed that total site density has no effect on the predicted mass fluxes. This can also be observed by directly using the steady state value of [(s)] into the rate equations. For a site density of $B = 1 \times 10^{-3}$ mol/m^2, the mass flux profiles using the unsteady approach starts to diverge from the steady state mass flux profiles after a total simulation time of 1.14×10^{-3} s. This results is shown on Fig. 12b.

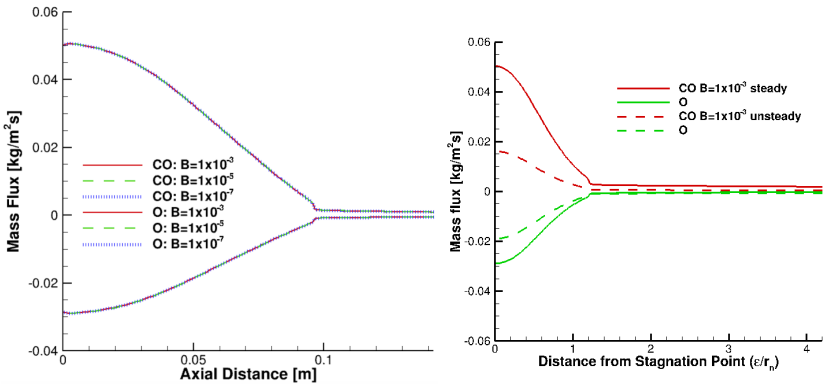

(a) Steady state

(b) Unsteady B $= 1 \times 10^{-3}$ mol/m^2 mass flux

Figure 12: *Mass flux of surface reacting species as a function of total site density B*

Using that time as a reference point, it is possible to evaluate the unsteady effects of the site density. On Fig. 13, it can be seen that a value of $B = 1 \times 10^{-5}$ mol/m^2 can be thought as the lower limit, where the steady-state equation can be used.

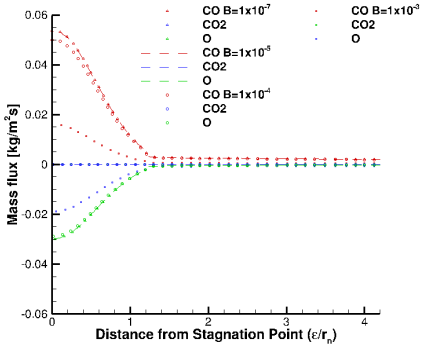

Figure 13: *Mass flux of surface reacting species as a function of total site density B*

2 Impacts

2.1 On the principal discipline(s) of the project

- Using the Kinetic Monte Carlo (kMC) method, we have simulated carbon oxidation with full atomic resolution at mesoscopic lengthscales ($10^2 - -10^3$ nanometers) and macroscopic timescales (up to seconds), based purely on elementary reaction rates derived from first principles. This allowed us to study in heretofore unattained detail the phenomenon of pitting, which is the structural evolution of the carbon surface as an intrinsic result of its oxidation process on the atomic level.
- The kMC model serves as the starting point for the development of pitting models used in macroscopic CFD calculations, thereby linking the true atomic scale surface chemistry to macroscopic phenomena in hypersonic aerothermodynamics.
- We are now able of model multilayer graphene and graphite, with arbitrary defect distributions. This allows us to calculate not only in-plane pitting rates in the surface layer, but also in-depth pitting rates across multiple layers.
- We have develop and implement a novel method (hinge method) for immersed boundaries that uses fluxes manipulation and avoid mesh movements and conformal meshes. The method can be used at the micro-scale or the macro-scale, and is validated for hypersonic flows.

2.2 On other disciplines

The result of Task B, in regards to the pit geometry being either circular (with rough edges) or hexagonal (with atomically smooth edges), is of interest to manufacturing of graphene nanodevices. For instance, graphene has been utilized experimentally in laboratory environments in the form of nanoporous graphene membranes for water desalination [32] and DNA sequencing [33, 34], as well as in the form of graphene nanoribbons (GNR) with open bandgaps that can be utilized as transistors [35, 36]. The function of such devices depends critically on the material structure at the atomic level. For example, the electric conductivity of GNR is controlled by the structure of graphene edges, where roughness or irregularity reduces the conductivity and therefore diminishes the desired function [37]. A promising technique that allows control over the edge structure at the atomic level is etching of graphene through oxidation in a gaseous environment at elevated temperatures [38], just like we have studied it. As we have shown, the resulting graphene edge structure can be both atomically smooth or rough based on temperature and pressure, which culminates in either hexagonal or circular etch figures [22, 23]. In the end, our work provides a firm theoretical basis for understanding and modeling oxidative etching, and we hope that this will support it as a manufacturing technique on the way to practical employment in research labs and industrial settings.

2.3 Human resources, teaching and educational experience

- Multiple undergraduate students were in involved in the project. Two of these ended up being co-authors on conference papers. One of these students is now pursuing a PhD at UIUC.
- The PhD student in charge of Task B, participated and won (in the College of Engineering) the Three Minute Thesis competition. A video of the talk can be found at the following link: https://www.youtube.com/watch?v=JpAFnhVF-3o

3 Changes

3.1 Changes in approach

3.2 Lit Review

In Task A, the approach was changed. A thorough literature survey revealed that the mechanisms necessary to put together the model had been previously published. Thus, these were used. DFT calculations were run for alternate mechanisms, but those ended up not being of importance to the model. These results were nevertheless published, they did not contribute directly to the project.

3.2.1 Carbon Nitridation

Task A was also extended to include Nitrogen reactions. Following the same approach as for carbon oxidation, we have compiled a kinetic mechanism for the nitrogen-carbon gas-surface reaction. As can be seen in Table 3, it contains the same types of elementary surface reactions as the oxidation mechanism. However, it is much less detailed, in particular in respect to CN formation reactions at different types of edge carbons, because studies on the energetics of carbon nitridation are rare. Nevertheless, we observe the same characteristic surface evolution, namely pitting of the carbon surface as a result of preferential removal of edge carbon atoms. Preliminary results on the pitting rates for nitridation are shown in Figure 14. Notice that the simulated pressures are high for atomic nitrogen, in contrast to the presented carbon oxidation data, where the pressures are given for air in chemical equilibrium, such that the atomic oxygen concentrations are many orders of magnitude lower.

Table 3: *Kinetic mechanism for nitrogen-carbon gas-surface reaction.*

Reaction	Energy Barrier E_a(eV)
N Adsorption	0.0
N Desorption	1.1
N_2 Recombinative Desorption	0.37
N_2 Eley-Rideal Desorption	0.0
N Diffusion	0.88
CN Formation	2.75

3.2.2 3D/Multilayer Pitting

For Task B, we have started to extend our simulation framework to multilayer graphene/graphite materials. The working assumption for now is that there are no chemical interactions between layers, so the only interlayer effect is the blocking off of lower layers from the impinging gas by the surface layer(s). This is partially due to the lack of data on the energetics of potential chemical interactions, but also due to the fact that the experimental results on this matter are inconclusive at best. We have performed simulations of multilayer pits, with initial monovacancies at the same location in each layer. Figure 15 shows simulation snapshots of two of those simulations. Snapshot a) corresponds to a reaction at high pressure and temperature, whereas b) corresponds to low pressure and temperature. We can measure and compare the pitting rates in-plane (as done before for single layer pitting) and in-depth (across layers). Figure 16 shows the ratio between those, as a function of reaction conditions. It becomes clear that at low pressure and temperature, the in-plane rate is several orders of magnitude faster than the in depth rate, which favors the

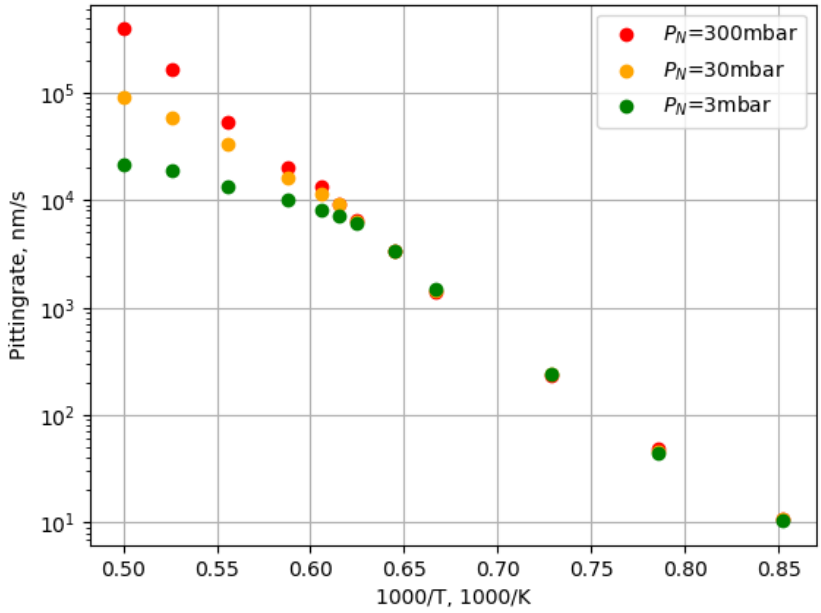

Figure 14: *Pit growth rates as a function of temperature and pressure for carbon nitridation.*

growth of shallow pits (layer by layer oxidation). In contrast, higher pressure and temperature cause a relative increase in the in-depth pitting rate, which favors the growth of deeper pits. We are working on extending those preliminary results to multilayer carbon materials with arbitrary defect distributions. For instance, we attached two supplemental videos SV3 and SV4, the former showing multilayer pitting with monovacancies in the same location as discussed here, the latter showing a random distribution of monovacancies in each layer. Movies of these simulations can be found at:

- https://youtu.be/J_aM12LZnh4
- https://youtu.be/om2zdyB3-Rc

3.3 Delay

- Co-PI (formerly PI) left in the middle of the project, and did not contributed since. The student in charge of Task A (Simon Schmidt) was, fortunately, far enough trained to be able to continue the project, graduate, and keep working on it as a postdoc. This has caused minor delays in the approach, but significant delays with regards to publications.
- The senior student that was tasked with helping implement the last few features in the code in Task C went back to his home country in January 2020, and was only able to renew his visa in September 2021. He was able to contribute to the project, but since he did not have great working conditions, he was not as efficient. The student that was in charge of Task B became sick with COVID for about 1 month, and was not able to work during that time.

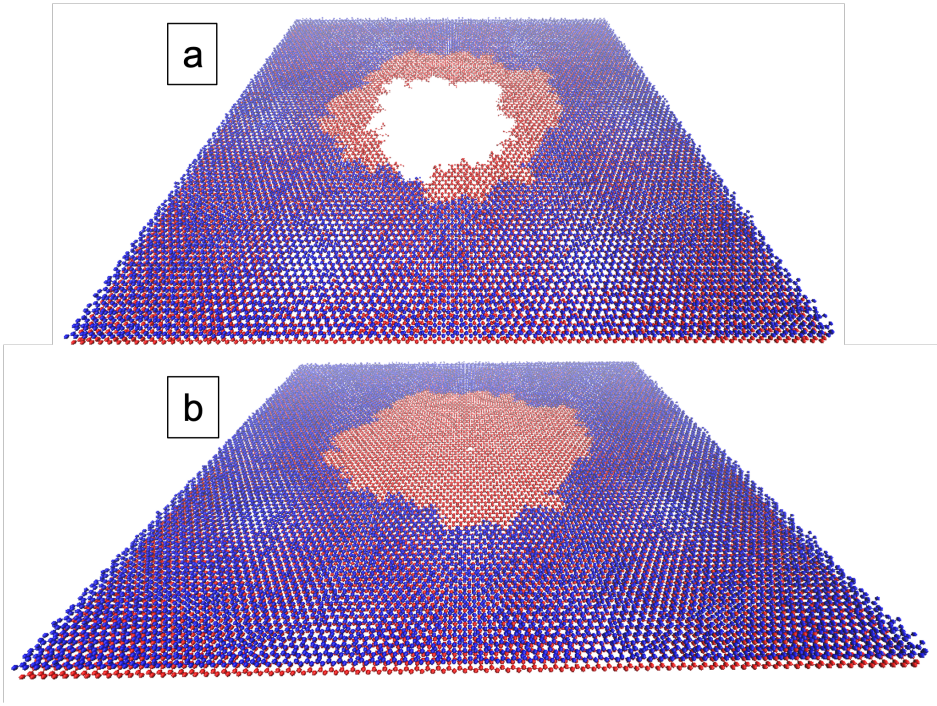

Figure 15: *Geometry comparison of simulated etch pits: (a) deep pit with in-depth pitting rate of similar magnitude to in-plane pitting rate; (b) shallow pit with in-depth pitting rate much smaller than in-plane pitting rate.*

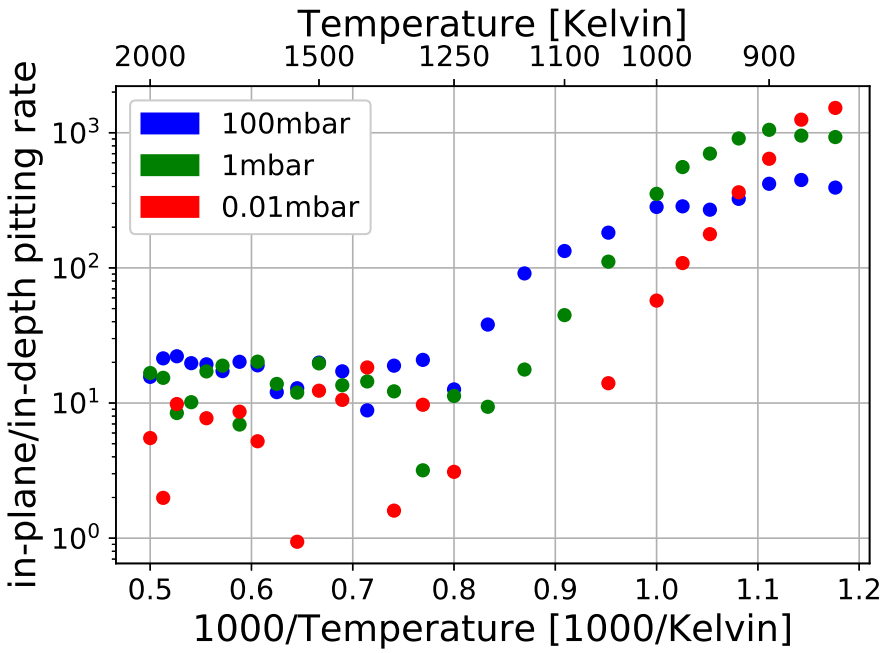

Figure 16: *Comparison of in-plane and in-depth pitting rates as a function of temperature and pressure.*

4 Technical Updates

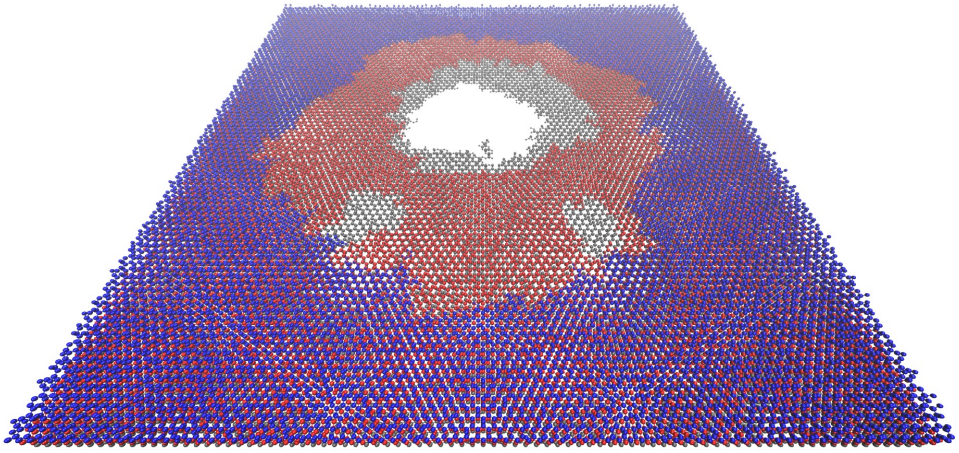

Figure 17: *Simulation of multilayer graphite, with arbitrary defect distributions, which allows the derivation of in-depth pitting rates across multiple atomic layers.*

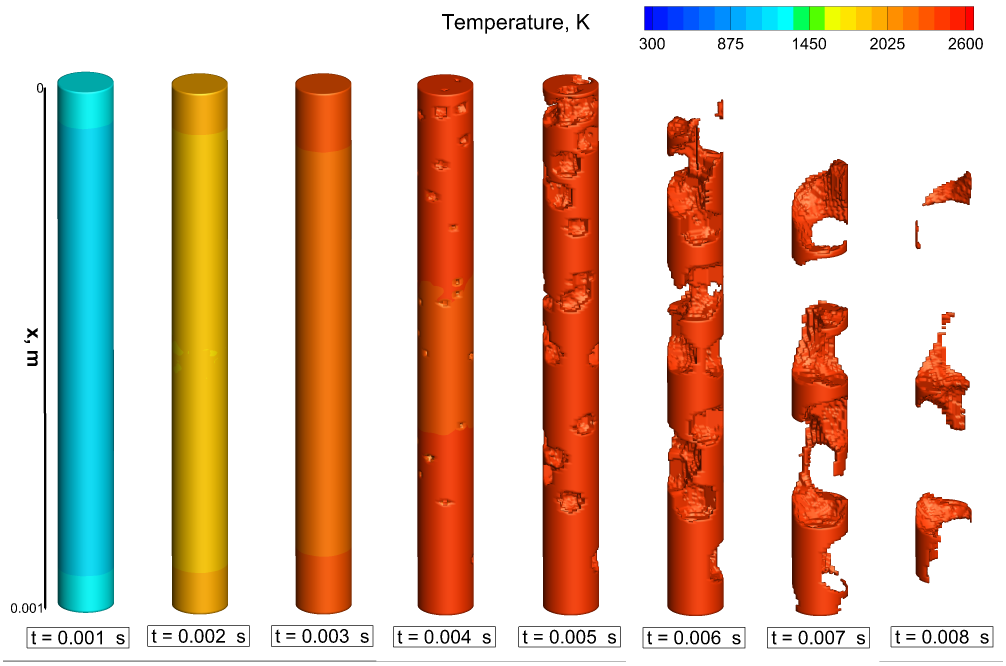

Figure 18: *Modeling of pits forming on a carbon fibers using pit formation rates extrapolated from first principles.*

References

[1] Ning Chen and Ralph T. Yang. Ab Initio Molecular Orbital Study of the Unified Mechanism and Pathways for Gas Carbon Reactions. *The Journal of Physical Chemistry A*, 102(31):6348–6356, 7 1998.

[2] Ning Chen and Ralph T. Yang. Ab initio molecular orbital calculation on graphite: Selection of molecular system and model chemistry. *Carbon*, 36(7-8):1061–1070, 1998.

[3] Jacob A. Moulijn and Freer Kapteijn. Towards a unified theory of reactions of carbon with oxygen-containing molecules. *Carbon*, 33(8):1155–1165, 1 1995.

[4] S. G. Chen, Ralph T. Yang, F. Kapteijn, and Jacob A. Moulijn. A New Surface Oxygen Complex on Carbon: Toward a Unified Mechanism for Carbon Gasification Reactions. *Industrial & Engineering Chemistry Research*, 32(11):2835–2840, 11 1993.

[5] Karina Sendt and Brian S. Haynes. Density functional study of the chemisorption of O$_2$ on the armchair surface of graphite. *Proceedings of the Combustion Institute*, 30(2):2141–2149, 1 2005.

[6] Karina Sendt and Brian S. Haynes. Density functional study of the chemisorption of O$_2$ on the zig-zag surface of graphite. *Combustion and Flame*, 143(4):629–643, 12 2005.

[7] Karina Sendt and Brian S. Haynes. Density Functional Study of the Reaction of Carbon Surface Oxides: The Behavior of Ketones. *The Journal of Physical Chemistry A*, 109(15):3438–3447, 4 2005.

[8] Karina Sendt and Brian S. Haynes. Modelling CO desorption from carbon chars using density functional theory. In *5th Asia-Pacific Conference on Combustion, ASPACC 2005: Celebrating Prof. Bob Bilger's 70th Birthday*, number January 2005, pages 121–124, 2005.

[9] Karina Sendt and Brian S. Haynes. Density Functional Study of the Chemisorption of O$_2$ Across Two Rings of the Armchair Surface of Graphite. *The Journal of Physical Chemistry C*, 111(14):5465–5473, 4 2007.

[10] Karina Sendt and Brian S. Haynes. Modelling Chemisorption of O 2 on Carbon Chars Using Density Functional Theory. In *Proceedings of the Australian Combustion Symposium*, 2007.

[11] Karina Sendt and Brian S. Haynes. Density functional study of the reaction of O$_2$ with a single site on the zigzag edge of graphene. *Proceedings of the Combustion Institute*, 33(2):1851–1858, 1 2011.

[12] Rosanna Larciprete, Stefano Fabris, Tao Sun, Paolo Lacovig, Alessandro Baraldi, and Silvano Lizzit. Dual Path Mechanism in the Thermal Reduction of Graphene Oxide. *Journal of the American Chemical Society*, 133(43):17315–17321, 11 2011.

[13] Rosanna Larciprete, Paolo Lacovig, Sandra Gardonio, Alessandro Baraldi, and Silvano Lizzit. Atomic Oxygen on Graphite: Chemical Characterization and Thermal Reduction. *The Journal of Physical Chemistry C*, 116(18):9900–9908, 5 2012.

[14] Alejandro Montoya, Thanh-Thai T. Truong, Fanor Mondragón, and Thanh N. Truong. CO Desorption from Oxygen Species on Carbonaceous Surface: 1. Effects of the Local Structure of the Active Site and the Surface Coverage. *The Journal of Physical Chemistry A*, 105(27):6757–6764, 7 2001.

[15] Alejandro Montoya, Fanor Mondragón, and Thanh N. Truong. First-Principles Kinetics of CO Desorption from Oxygen Species on Carbonaceous Surface. *The Journal of Physical Chemistry A*, 106(16):4236–4239, 4 2002.

[16] Alejandro Montoya, Fanor Mondragón, and Thanh N. Truong. CO$_2$ adsorption on carbonaceous surfaces: a combined experimental and theoretical study. *Carbon*, 41(1):29–39, 1 2003.

[17] Željko Šljivančanin, Aleksandar S. Milošević, Zoran S. Popović, and Filip R. Vukajlović. Binding of atomic oxygen on graphene from small epoxy clusters to a fully oxidized surface. *Carbon*, 54:482–488, 2013.

[18] J. Brunner and H. Hammerschmid. Zur Morphologie des Graphits. *Zeitschrift für anorganische und allgemeine Chemie*, 155(1):255–256, 7 1926.

[19] Arthur F. Voter. Introduction to the Kinetic Monte Carlo Method. In *Radiation Effects in Solids*, pages 1–23. Springer Netherlands, Dordrecht, 2007.

[20] Jens Nielsen, Mayeul D'Avezac, James Hetherington, and Michail Stamatakis. Parallel kinetic Monte Carlo simulation framework incorporating accurate models of adsorbate lateral interactions. *The Journal of Chemical Physics*, 139(22):224706, 12 2013.

[21] Michail Stamatakis, Ying Chen, and Dionisios G. Vlachos. First-Principles-Based Kinetic Monte Carlo Simulation of the Structure Sensitivity of the Water-Gas Shift Reaction on Platinum Surfaces. *The Journal of Physical Chemistry C*, 115(50):24750–24762, 12 2011.

[22] Arnaud Delehouzé, Francis Rebillat, Patrick Weisbecker, Jean-Marc Leyssale, Jean-Francois Epherre, Christine Labrugère, and Gerard L. Vignoles. Temperature induced transition from hexagonal to circular pits in graphite oxidation by O$_2$. *Applied Physics Letters*, 99(4):044102, 7 2011.

[23] Joachim Dahl Thomsen, Jens Kling, David M. A. Mackenzie, Peter Bøggild, and Timothy J. Booth. Oxidation of Suspended Graphene: Etch Dynamics and Stability Beyond 1000 °C. *ACS Nano*, 13:acsnano.8b08979, 1 2019.

[24] Florian Oberhuber. *Untersuchung kristallographisch definierter Graphen-Ränder*. PhD thesis, Universität Regensburg, 2015.

[25] Gergely Dobrik, Levente Tapasztó, and László Peter Biró. Selective etching of armchair edges in graphite. *Carbon*, 56:332–338, 5 2013.

[26] J. R. Hahn. Kinetic study of graphite oxidation along two lattice directions. *Carbon*, 43(7):1506–1511, 6 2005.

[27] J. R. Hahn, H. Kang, Seung Mi Lee, and Young Hee Lee. Mechanistic Study of Defect-Induced Oxidation of Graphite. *The Journal of Physical Chemistry B*, 103(45):9944–9951, 11 1999.

[28] Umran Duzel. *Development of Universal Solver for High Enthalpy Flows Through Ablative Materials*. Ph.D. Thesis, University of Kentucky, Lexington, KY, December 2020.

[29] Ümran Düzel, Olivia M. Schroeder, Huaibao Zhang, and Alexandre Martin. Numerical simulation of an arc jet test section. *Journal of Thermophysics and Heat Transfer*, 34(2):393–403, April 2020.

[30] Savio Poovathingal, Thomas E. Schwartzentruber, Vanessa J. Murray, Timothy K. Minton, and Graham V. Candler. Finite-rate oxidation model for carbon surfaces from molecular beam experiments. *AIAA Journal*, 55(5):1644–1658, 2017.

[31] George Blyholder and Henry Eyring. Kinetics of graphite oxidation. *The Journal of Physical Chemistry*, 61(5):682–688, 1957.

[32] Sumedh P. Surwade, Sergei N. Smirnov, Ivan V. Vlassiouk, Raymond R. Unocic, Gabriel M. Veith, Sheng Dai, and Shannon M. Mahurin. Water desalination using nanoporous single-layer graphene. *Nature Nanotechnology*, 10(5):459–464, 5 2015.

[33] Gregory F. Schneider, Stefan W. Kowalczyk, Victor E. Calado, Gregory Pandraud, Henny W. Zandbergen, Lieven M. K. Vandersypen, and Cees Dekker. DNA Translocation through Graphene Nanopores. *Nano Letters*, 10(8):3163–3167, 8 2010.

[34] Stephanie J. Heerema and Cees Dekker. Graphene nanodevices for DNA sequencing. *Nature Nanotechnology*, 11(2):127–136, 2 2016.

[35] Amir Kaplan, Zhe Yuan, Jesse D. Benck, Ananth Govind Rajan, Ximo S. Chu, Qing Hua Wang, and Michael S. Strano. Current and future directions in electron transfer chemistry of graphene. *Chemical Society Reviews*, 46(15):4530–4571, 2017.

[36] Frank Schwierz. Graphene transistors. *Nature Nanotechnology*, 5(7):487–496, 2010.

[37] Rajesh Kumar, Sumanta Sahoo, Ednan Joanni, Rajesh Kumar Singh, Wai Kian Tan, Kamal Krishna Kar, and Atsunori Matsuda. Recent progress in the synthesis of graphene and derived materials for next generation electrodes of high performance lithium ion batteries. *Progress in Energy and Combustion Science*, 75:100786, 11 2019.

[38] László Peter Biró, Peter Nemes-Incze, and Philippe Lambin. Graphene: nanoscale processing and recent applications. *Nanoscale*, 4(6):1824–1839, 2012.

REQUEST FOR ADVANCE OR REIMBURSEMENT

(See instructions on back)

OMB APPROVAL NO. 0348-0004

PAGE 1 OF 1 PAGES

1. TYPE OF PAYMENT REQUESTED
   a. "X" one or both boxes: [ ] Advance [X] Reimbursement
   b. "X" the applicable box: [X] FINAL [ ] PARTIAL

2. BASIS OF REQUEST: [ ] CASH [X] ACCRUAL

3. FEDERAL SPONSORING AGENCY AND ORGANIZATION ELEMENT TO WHICH THIS REPORT IS SUBMITTED	4. FEDERAL GRANT OR OTHER IDENTIFYING NUMBER ASSIGNED BY FEDERAL AGENCY	5. PARTIAL PAYMENT REQUEST NUMBER FOR THIS REQUEST
Air Force Office of Scientific Research	FA9550-18-1-0261	P100119947-Final

6. EMPLOYER IDENTIFICATION NUMBER	7. RECIPIENT ACCOUNT NUMBER OR IDENTIFYING NUMBER	8. PERIOD COVERED BY THIS REQUEST	
		FROM (month, day, year)	TO (month, day, year)
1616033693A1	3200002041	8/15/2020	8/14/2021

9. Recipient Organization
Name: University of Kentucky Research Foundation
Number and Street: Kinkead Hall
City, State and ZIP Code: Lexington, KY 40506-0057

10. PAYEE (Where check is to be sent if different than item 9)
Name: **University of Kentucky Research Foundation**
Number and Street: **c/o National City Bank**
PO Box 931113
City, State and ZIP Code: **Cleveland, OH 44193**

11. COMPUTATION OF AMOUNT OF REIMBURSEMENTS/ADVANCES REQUESTED

PROGRAMS/FUNCTIONS/ACTIVITIES		(a)	(b)	(c)	(d) TOTAL
a. Total program outlays to date	(As of date) 8/14/2021	$510,590.99	$0.00	$0.00	$510,590.99
b. Less: Cumulative program income		$0.00	$0.00	$0.00	$0.00
c. Net program outlays (*Line a minus line b*)		$510,590.99	$0.00	$0.00	$510,590.99
d. Estimated net cash outlays for advance period		$0.00	$0.00	$0.00	$0.00
e. Total (*Sum of lines c & d*)		$510,590.99	$0.00	$0.00	$510,590.99
f. Non-Federal share of amount on line e		$0.00	$0.00	$0.00	$0.00
g. Federal share of amount on line e		$510,590.99	$0.00	$0.00	$510,590.99
h. Federal payments previously requested		$321,736.01	$0.00	$0.00	$321,736.01
i. Federal share now requested (*Line g minus line h*)		$188,854.98	$0.00	$0.00	$188,854.98
j. Advances required by month, when requested by Federal grantor agency for use in making prescheduled advances	1st month				
	2nd month				
	3rd month				

12. ALTERNATE COMPUTATION FOR ADVANCES ONLY

a. Estimated Federal cash outlays that will be made during period covered by the advance	
b. Less: Estimated balance of Federal cash on hand as of beginning of advance period	
c. Amount requested (Line a minus line b)	

13. CERTIFICATION

I certify that to the best of my knowledge and belief the data on the reverse are correct and that all outlays were made in accordance with the grant conditions or other agreement and that payment is due and has not been previously requested.

SIGNATURE OF AUTHORIZED CERTIFYING: Jessica Milner on behalf of Paige Brown

DATE REQUEST SUBMITTED:

TYPED OR PRINTED NAME AND TITLE: Paige G. Brown, Director, Research Financial Services

TELEPHONE (AREA CODE, NUMBER, EXTENSION): (859)257-3662

This space for agency use

University of Kentucky

THE UNIVERSITY OF KENTUCKY RESEARCH FOUNDATION

INVOICE

To: **US Air Force Office of Scientific Research**
PO Box 7020
Bellevue, NE 68005-1920

THE FOLLOWING MUST BE REFERENCED ON THE PAYMENT FOR CREDIT TO THE PROPER ACCOUNT:

Invoice No.	:	P100119947-Final
Invoice Amt.	:	**$ 188,854.98**
Invoice Period	:	08/15/2020 - 08/14/2021
Date	:	11/11/2021
Account No.	:	3200002041
Tax ID No.	:	61-6033693

Project Title: CARBON OXIDATION IN EXTREME ENVIRONMENTS

Prin. Investigator: MARTIN ALEXANDRE
Reference: FA9550-18-1-0261
Budget Period: 08/15/2018-08/14/2021
Award: $511,281.00

REMIT: **Preferred Payment method:**
ACH electronic funds transfer
If ACH is not available for your organization, payments should be made to:
University of Kentucky Research Foundation
c/o PNC Bank
PO Box 931113
Cleveland, OH 44193

Invoice Details - Amounts in USD

	Current Expenses	Cumulative Expenses
SALARIES	**98,422.13**	257,038.60
BENEFITS	**16,565.57**	40,849.20
TRAVEL	**0.00**	14,299.73
SERVICES	**515.00**	515.00
TUITION & FEES	**12,136.00**	32,156.25
FAC & ADMIN EXPENSE	**61,216.28**	165,732.21
TOTAL------>	**188,854.98**	510,590.99

By signing this report, I certify to the best of my knowledge and belief that the report is true, complete, and accurate, and the expenditures, disbursements and cash receipts are for the purposes and objectives set forth in the terms and conditions of the Federal award. I am aware that any false, fictitious, or fraudulent information, or the omission of any material fact, may subject me to criminal, civil, or administrative penalties for fraud, false statements, false claims or otherwise. (U.S. Code Title 18, Section 1001 and Title 31, Sections 3729-3730 and 3801-3812).

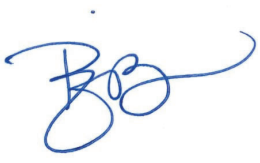

Paige G. Brown, Director, Research Financial Services
(859) 257-3662
FA ID: JLCHAP4
Print ID: LOIS

FEDERAL FINANCIAL REPORT

(Follow form instructions)

1. Federal Agency and Organizational Element to Which Report is Submitted	2. Federal Grant or Other Identifying Number Assigned by Federal Agency (To report multiple grants, use FFR Attachment)	Page 1 of 1 pages
US Air Force Office of Scientific Research	FA9550-18-1-0261	

3. Recipient Organization (Name and complete address including Zip code)
University of Kentucky Research Foundation
c/o PNC Bank
PO Box 931113
Cleveland, OH 44193

4a. DUNS Number	4b. EIN	5. Recipient Account Number or Identifying Number (To report multiple grants, use FFR Attachment)	6. Report Type	7. Basis of Accounting
939017877	61-6033693	3200002041	X Final	□ Cash X Accrual

8. Project/Grant Period From: (Month, Day, Year)	To: (Month, Day, Year)	9. Reporting Period End Date (Month, Day, Year)
8/15/2018	8/14/2021	8/14/2021

10. **Transactions**	Cumulative
(Use lines a-c for single or multiple grant reporting)	
Federal Cash (To report multiple grants, also use FFR Attachment):	
a. Cash Receipts	$321,736.01
b. Cash Disbursements	$510,590.99
c. Cash on Hand (line a minus b)	($188,854.98)
(Use lines d-o for single grant reporting)	
Federal Expenditures and Unobligated Balance:	
d. Total Federal funds authorized	$511,281.00
e. Federal share of expenditures	$510,590.99
f. Federal share of unliquidated obligations	$0.00
g. Total Federal share (sum of lines e and f)	$510,590.99
h. Unobligated balance of Federal funds (line d minus g)	$690.01
Recipient Share:	
i. Total recipient share required	$0.00
j. Recipient share of expenditures	$0.00
k. Remaining recipient share to be provided (line i minus j)	$0.00
Program Income:	
l. Total Federal program income earned	$0.00
m. Program income expended in accordance with the deduction alternative	$0.00
n. Program income expended in accordance with the addition alternative	$0.00
o. Unexpended program income (line l minus line m or line n)	$0.00

	a. Type	b. Rate	c. Period From	Period To	d. Base	e. Amount Charged	f. Federal Share
11. Indirect Expense	Predetermined	53%	8/15/2018	8/14/2021	$115,602.70	$61,216.28	$61,216.28
				g. Totals:	$115,602.70	$61,216.28	$61,216.28

12. *Remarks: Attach any explanations deemed necessary or information required by Federal sponsoring agency in compliance with governing legislation:*
ELECT TO CARRY FORWARD THE REMAINING BALANCE IN LINE h.

13. Certification: By signing this report, I certify that it is true, complete, and accurate to the best of my knowledge. I am aware that any false, fictitious, or fraudulent information may subject me to criminal, civil, or administrative penalties. (U.S. Code, Title 18, Section 1001)

a. Typed or Printed Name and Title of Authorized Certifying Official	c. Telephone (Area code, number and extension)
Paige G. Brown, Director, Research Financial Services	(859) 257-3662
	d. Email address: UKRFInvoices@uky.edu
b. Signature of Authorized Certifying Official: Jessica Milner on behalf of Paige Brown	e. Date Report Submitted (Month, Day, Year)
	14. Agency use only:

Standard Form 425
OMB Approval Number: 0348-0061
Expiration Date: 10/31/2011

LT

From: Air Force Office of Scientific Research
To: Technical Reports
Subject: [Non-DoD Source] Deliverable Received: FA9550-18-1-0261
Date: Sunday, November 14, 2021 11:35:44 PM

OMA Team,
A new Final Performance has been submitted for your attention. Award Number: FA9550-18-1-0261

Supporting Report: https://afosr.gov1.qualtrics.com/WRQualtricsSurveyEngine/File.php?F=F_1luz0gYhRaatnwt

- Date Stamp: 23:33:20 , 11/14/2021
- Title: Carbon oxidation in extreme environments
- DISTRIBUTION: Yes- Approved for Public Release (Distro A)
- Principal Investigator: MARTIN, ALEXANDRE
  - PI Email: alexandre.martin@uky.edu
- Program Officer: POPKIN, SARAH
- Report Type: Final Performance
- Reporting Period
  - Start Date: 08/15/2018
  - End Date: 08/14/2021
- Award Number: FA9550-18-1-0261
- Report Due Date: 11/12/2021

ABSTRACT:
Hypersonic aircrafts must be protected from the extremely high temperatures of the gas impinging their surface. This is achieve by using Thermal Protection Systems (TPS), which typically consist of a thin coating layer made of a very resistant material that stands well these high temperatures. One of the most versatile materials used for this purpose is carbon, in some of its many possible forms, such as graphite, glassy or amorphous. However, in the presence of high temperature oxygen, as is the case during flight, the carbon layer of the TPS degrades and the solid carbon become gaseous CO and CO2. As a result, the protective layer may eventually disappear, leaving the vehicle without protection. Thus, a good understanding of its behavior under these conditions is very important to improve the safety of hypersonic flights. The guiding idea of this project is to study carbon oxidation in these extreme conditions, from a fundamental point of view. This will be achieved by examining the details of the atomic-scale processes that ultimately govern the loss of carbon from the TPS. After hitting the surface, oxygen atoms remain wandering across the TPS surface until they connect to weakly attached carbon atoms . Oxygen and carbon then combine and eventually leave the surface as CO or CO2. These processes are very difficult to study experimentally because of the scales of a few Angstroms. Instead, we will use Quantum Mechanics calculations to study all these processes. This will help to develop models of carbon oxidation, which will then be used in

large scale Computational Fluid Dynamics codes to simulate the gas flow around hypersonic aircrafts. We are specifically interested in the accurate prediction of the TPS loss of carbon, with the ultimate goal of contributing to improve safety.